Biophysical Journal
Article

Biophysical Society

Bending moduli of mixtures: Diffusional softening and interactions

Lucy Knox,[1] Peter Winstel,[1] Markus Deserno,[1] John F. Nagle,[1,*] and Stephanie Tristram-Nagle[1,*]
[1]Physics Department, Carnegie Mellon University, Pittsburgh, Pennsylvania

ABSTRACT The apparent bending moduli (K_C) of bilayers composed of binary mixtures of lipids with different spontaneous curvatures have been obtained using x-ray diffuse scattering (XDS). The mixtures that were studied are POPC/POPE, POPC/POPA, POPC/POPS, and DLPC/DiPhyPC. The data are qualitatively consistent with what is expected from the theory of diffusional softening for lipids with different spontaneous curvatures. However, the derived spontaneous curvature differences are larger than those obtained from the hexagonal$_{II}$ (H_{II}) phase and from a recent giant unilamellar vesicle (GUV) study. We propose that the interactions between lipids, which we have added to the theory, also play an important role in the values of K_C obtained at the short length scale of XDS. Inclusion of a mean field term in the analysis brings the calculated difference in spontaneous curvatures ΔC_0 of the two lipids closer to the values from the H_{II} and GUV methods. The use of XDS opens a new experimental window on diffusional softening and the interactions between lipids in mixtures.

SIGNIFICANCE Lipid curvature is significant because it is a fundamental property of biological membranes that drives essential cellular processes such as vesicle fusion, cell signaling, and membrane protein function. The intrinsic shape of lipids determines their ability to bend, influencing membrane structure and the formation of lipid rafts. We introduce the use of x-ray diffuse scattering (XDS), which demonstrates decreased bending moduli when mixing two lipids with different spontaneous curvatures. By fitting the data with diffusional softening equations modified by a mean field approach to lipid-lipid interactions, we obtain differences in lipid spontaneous curvatures consistent with those previously reported using hexagonal$_{II}$ phases and giant unilamellar vesicles. We suggest that XDS measurements at short wavelengths provide insights into lipid-lipid interactions that determine mechanical properties.

INTRODUCTION

As biomembranes have many lipid components, it is of general interest to learn which aspects of their mixing affect their structural and mechanical properties, and the study of binary lipid mixtures is fundamental to this. To first approximation, the properties of a mixture linearly change as the mole fraction $\overline{\phi}$ of a second component increases; indeed, our lab has observed linear increases in volumes when two phosphatidylcholine lipids were added together (1) (S.T.-N. unpublished data). However, deviations are generally expected, and observed, in the case of adding cholesterol even for volumes (2), and for areas, thicknesses, and the bending modulus K_C (3), which is the mechanical property we focus on in this paper. Although we have found nearly linear structural properties such as volume for various non-cholesterol pairs of lipids (1), this is not the case for the bending modulus data that are presented in this paper.

Curvature elasticity of lipid membranes is described by the familiar Helfrich-Canham expression

$$E_{HC} = \frac{1}{2}K_C \int [C(\boldsymbol{r}) - C_0]^2 \, d^2r, \qquad (1)$$

where $C(\boldsymbol{r})$ is the total membrane curvature at lateral position $\boldsymbol{r}$, and K_C is the bending modulus. The parameter C_0 is the spontaneous bilayer curvature, i.e., the preferred value of $C(\boldsymbol{r})$ at which the bending energy vanishes. For single-component membranes this is necessarily zero, because the intrinsic lipid curvatures in the two leaflets cancel by symmetry. However, each leaflet of a bilayer is described by a curvature elastic expression similar to Eq. 1 in which the spontaneous curvature is that of the individual monolayer, and as such has a generally non-zero value that depends on lipid species.

Submitted September 23, 2025, and accepted for publication December 29, 2025.

Correspondence:*Correspondence: nagle@cmu.edu or stn@cmu.edu

Editor: Edward Lyman.
https://doi.org/10.1016/j.bpj.2025.12.037

Thus, the natural context for intrinsic lipid curvature, as originally discussed (4), is the spontaneous monolayer curvature of a single leaflet. This makes the situation more interesting for mixed membranes, since the lipid compositions in both leaflets can fluctuate independently from one another, and local leaflet spontaneous curvatures are no longer guaranteed to cancel. Hence, C_0 becomes a position-dependent field, $C_0(\boldsymbol{r})$, whose fluctuations couple to membrane shape via Eq. 1. The resulting possibility of correlated shape-composition fluctuations, also described as curvature-composition coupling (5,6), gives rise to the effect of diffusional softening: shape undulations $C(\boldsymbol{r})$ that happen to match local spontaneous curvature fluctuation $C_0(\boldsymbol{r})$ have a lower energy and, hence, a larger statistical weight. Overall, this ends up increasing the mean squared amplitudes of observed shape undulations, as in Fig. 1, which in turn is perceived as a softened bending modulus by x-ray diffuse scattering (XDS) and by shape analysis of giant unilamellar vesicles (GUVs). While Fig. 1 might be taken to suggest that the undulations in Fig. 1 *A* occur first, followed by lipid diffusion in Fig. 1 *B*, we emphasize that XDS and typical GUV shape analysis obtain an ensemble of snapshots at equilibrium. These do not contain such dynamical information, so the theory that we shall relate to is an equilibrium statistical mechanical theory that couples the free energy of undulation fluctuations and the free energy of composition fluctuations to produce ensembles of snapshots for comparison to experiments.

As is well known, when the intrinsic curvature of lipids is large, amphiphiles do not form bilayer phases (4). If the intrinsic curvature is strongly negative, such as in 1,2-dioleoyl-*sn*-glycero-3-phosphatidylethanolamine (DOPE), an inverse hexagonal$_{\mathrm{II}}$ ($\mathrm{H_{II}}$) phase may form, after which the intrinsic lipid curvature is obtained from the structure of the $\mathrm{H_{II}}$ phase. In an important series of papers, Parsegian, Rand, Gruner, and co-workers (7–10) realized that addition of another lipid to the DOPE $\mathrm{H_{II}}$ phase changes the structure obtained by x-rays in a way that allows calculation of the spontaneous curvature difference ΔC_0 between the other lipid and DOPE. This has become the classical way of measuring intrinsic lipid curvature. It must be mentioned, however, that the sum of the curvature differences of lipid A in host B and lipid B in host C need not be the same as the difference between A in host C (11–13). The curvature difference between A in host B may even depend upon the concentration of A as reported in (14), so a well-defined scale of intrinsic curvatures for lipids may be problematic.

Leibler first described how inclusions with substantially different curvature from that of the host lipids would decrease the bilayer bending modulus (15). This idea has since been pursued by papers in the context of proteins or other non-lipid inclusions (16–19). Other studies have focused on mixtures of lipids, i.e., the effect of including a second lipid species, especially one with different intrinsic curvature. Bending moduli consistent with diffusional softening have been observed in mixed lipid membranes, both in molecular dynamics (MD) simulations (11,12,20–24) and in experiments using GUVs (25,26). However, some studies—both simulations (27–29) and experiments (30)—have reported K_{C} values for binary mixtures that are not consistent with diffusional softening. Furthermore, we have found no experimental references that report results for the complete range from one single lipid to the other single lipid, usually because the added lipid (e.g., DOPE or cholesterol) does not form bilayers. Sampling the entire range of mole fraction $\overline{\phi}$ from 0 to 1 is necessary to assure that a decrease in K_{C} is not just due to linear additivity of a lipid with small intrinsic K_{C}, and a longer range of compositions provides more precision. Accordingly, we have chosen to measure several mixtures that form bilayers over the full range of $\overline{\phi}$ from 0 to 1.

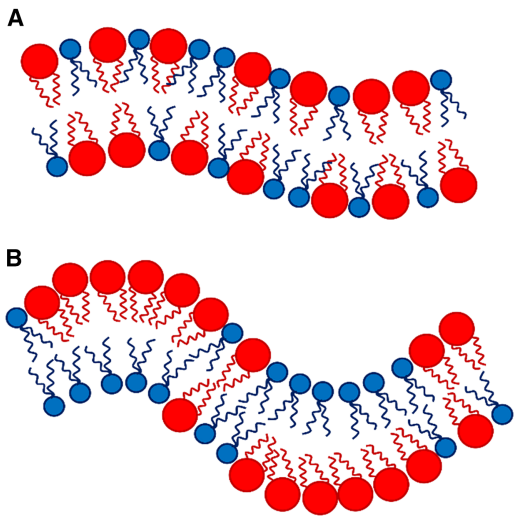

FIGURE 1 Sketch showing (*A*) a random mixture of positively curved lipids (*red*) and negatively curved lipids (*blue*) in a fluid, fluctuating bilayer. (*B*) The same bilayer in a configuration where local intrinsic curvature matches the curvature of the bilayer fluctuations. This favorable composition-shape correlation increases the height of the fluctuations, which decreases the observed bending modulus of the mixture.

MATERIALS AND METHODS

Materials

Lipids 1-palmitoyl-2-oleoyl-*sn*-glycero-3-phosphocholine (POPC), 1-palmitoyl-2-oleoyl-*sn*-glycero-3-phosphoethanolamine (POPE), 1-palmitoyl-2-oleoyl-*sn*-glycero-3-phospho-L-serine sodium salt (POPS), 1-palmitoyl-2-oleoyl-*sn*-glycero-3-phosphate sodium salt (POPA), 1,2-dilauroyl-*sn*-glycero-3-phosphocholine (DLPC), and 1,2-diphytanoyl-*sn*-glycero-3-phosphocholine (DiPhyPC) were purchased from Avanti Polar Lipids (Alabaster, AL) in lyophilized form and used as received. HPLC-grade organic solvents were purchased from Sigma-Aldrich (St. Louis, MO).

Methods

Sample preparation

Samples consisting of oriented stacks of ≈1800 bilayers were prepared using the "rock and roll" method (31). Four milligrams of lipid were

dissolved in organic solvent in glass vials (Agilent, Santa Clara, CA). The choice of organic solvent depended on the lipid mixture: chloroform/toluene (2:1, v/v; 3:1, v/v) or toluene/trifluoroethanol (1:1, v/v) for POPC/POPS, chloroform/trifluoroethanol (5:1, v/v) for DLPC/DiPhyPC or 2:1 (v/v) for POPC/POPA, and chloroform/hexafluoroisopropanol (1:2, v/v) for POPC/POPE. Samples were prepared by mixing known amounts of the pure lipids in 1:0, 2:1, 1:1, 1:2, and 0:1 molar ratios into small glass test tubes. The solution was vortexed and then plated onto a silicon wafer (15 mm width × 30 mm length × 1 mm height) inside a fume hood. The wafer was rocked while the organic solvent evaporated, producing an immobile, well-oriented film. After the film was formed in the hood, the sample was left to finish drying under vacuum for at least 2 h. The dried lipid was then trimmed to a 5-mm-wide by 30-mm-long strip along the center of the silicon wafer. The silicon wafer was fixed to a glass block (10 mm height × 15 mm width × 32 mm length) using heat sink compound (Dow Corning, Freeland, MI) and stored in a refrigerator at 4°C. At the time of x-ray data collection, samples were quickly transferred from a refrigerator to an insulated hydration chamber held at 37°C, which caused 100% hydration through the vapor within 10 min (32). In some cases, hydration was then lowered by flowing nitrogen into the chamber for 10 min followed by 10 min of equilibration.

Data collection

Low-angle x-ray scattering (LAXS) data were obtained at the ID7B2 line at the Center for High Energy X-ray Sciences (CHEXS, Ithaca, NY) on two separate trips to the Cornell High Energy Synchrotron Source (CHESS, Ithaca, NY) using an x-ray wavelength of 0.8856 Å, beam size 0.35 mm vertical × 0.26 mm horizontal, and sample-to-detector Eiger 16 M (Dectris, Baden, Switzerland) at distances of 400.1 mm and 348.0 mm. During each exposure, the sample was rotated from −1.0° to 6.0° over 15 s of x-irradiation or 0° to 5.0° over 10 s of x-irradiation. The background was collected by setting the x-ray angle of incidence to −2°, where sample scattering does not contribute to the image. Temperature was 37°C for all samples.

Data analysis

The background was subtracted from the scattering data to remove air and mylar scattering. Background due to water scattering was further removed by horizontal interpolation from outside the region of bilayer scattering. See Fig. S1 for an example of the subtracted XDS data. The scattering data were fit using the NFIT program (version 12.0.5). NFIT analyzes "lobes" of diffuse x-ray scattering data that are produced by membrane fluctuations in hydrated samples (33). It obtains the values of the bending modulus K_C and the compression modulus B from the best fit to the data of the calculated scattering from smectic liquid crystal theory defined by its free energy functional (34,35),

$$f = \frac{\pi}{2NL^2}\int_0^L rdr\sum_{n=0}^{N-1}\Big(K_C\left[\Delta_r^2 u_n(r)\right]^2 + B\left[u_{n+1}(r) - u_n(r)\right]^2\Big), \quad (2)$$

where u_n is the vertical membrane displacement of the nth bilayer in the stack of bilayers in our samples. The K_C term in Eq. 2 is the Helfrich-Canham curvature squared term in Eq. 1 with C_0 equal to 0 for symmetric bilayers. It is the modulus that is directly measured in static deformation studies such as electrodeformation (36), micropipette aspiration (37), and pulling tethers (38,39). XDS accumulates many snapshots on the photon femtosecond timescale that provide the equilibrium mean square correlation functions from which the static Helfrich-Canham bending modulus K_C is derivable using Eq. 2. (GUV shape analysis similarly obtains mean square fluctuations and derives K_C using Eq. 1.) The XDS intensity has two factors, a structure factor, $S(\mathbf{q})$, that depends upon the full scattering vector $\mathbf{q} = (q_r, q_z)$, and the square of the form factor, $F(q_z)$, that only depends upon q_z when the electron density depends only upon the distance along the normal z of the bilayer. The coherence of the beam limits the number of bilayers N and the effective lateral size L_r (40). The B term in Eq. 2 accounts for interactions between neighboring bilayers in the stack. The attractive van der Waals and repulsive hydration and undulation forces balance at a finite repeat D spacing of the order 50–80 Å depending upon the mixture. Charged lipids add an electrostatic repulsive interaction; this causes the D spacing to become infinite beyond a threshold concentration of charged lipid when there is sufficient water in our samples, which had counterions only. Therefore, the vapor pressure of water was maintained slightly below full hydration, as described previously, to maintain oriented stacks with D spacings of the order 100–200 Å. K_C and B were obtained for each of 3–9 accumulated images. These are usually obtained at slightly different hydration levels, but previous work has shown that this only affects B and not K_C as long as there is enough water for diffuse scattering (41). Average K_C and estimated uncertainty were then obtained for each mixture.

Theory

The theory of diffusional softening predicts that the effective bending modulus K_C belonging to the observed thermal undulations of a mixed membrane is smaller than a separate modulus K_D that would be obtained if there were no lateral diffusion. In particular, K_D is the bending modulus that would be measured by an experimental technique that dynamically examines membrane fluctuations on a timescale too short for the compositional degrees of freedom to also sample their thermal equilibrium distribution when diffusion is too slow compared to shape relaxation. Neutron spin echo (NSE) has been cited (22) as such a technique, although it has recently been shown that NSE data for cholesterol in DOPC is equally well accounted for by increased viscosity of the undulational modes (42).

Diffusional softening is then the result of isolating the thermal statistics of shape fluctuations in a membrane that has one shape and two composition fields (one for each leaflet). In the supporting material, we show that this leads to a bending modulus K_C that is softer than the dynamic modulus K_D:

$$\frac{K_C}{K_D} = \frac{1}{1+\alpha}, \quad (3)$$

where the softening constant α is itself proportional to K_D and given by

$$\alpha(\overline{\phi}) = \frac{K_D \Delta C_0^2 A_L \overline{\phi}\,(1-\overline{\phi})}{2k_B T(1 - 2\chi_{MF}\overline{\phi}\,(1-\overline{\phi}))}. \quad (4)$$

Here, ΔC_0^2 is the squared difference between the intrinsic curvatures of the two lipids, A_L is the interpolated area per lipid, $k_B T$ is the thermal energy, and $\overline{\phi}$ is the lipid mole fraction of the added second lipid species. Our current expressions generalize the theory as presented by Sapp et al. (25) in three ways. First, the right-hand side of Eq. 3 is not approximated by $1-\alpha$, as that is only true for small intrinsic curvature differences and anyway is unnecessary. Second, Eq. 4 includes the effect of non-ideal mixing at the level of a dimensionless mean-field mixing parameter χ_{MF}: a positive value for χ_{MF} favors like over unlike neighbors, with $\chi_{MF} > 2$ leading to lipid phase separation. Observe that $\chi_{MF} > 0$ enhances the effect of softening. Third, an explicit argument is given in the derivation in the supporting material for K_D having the form

$$K_D(\overline{\phi}) = (1-\overline{\phi})K_{C,1} + \overline{\phi}\,K_{C,2}, \quad (5)$$

where $K_{C,1}$ and $K_{C,2}$ are the measured values of pure lipids 1 and 2, respectively. It is encouraging that Fig. S4 in (43) shows linear plots for K_D over the full range of compositions of several mixtures, consistent with Eq. 5.

Eqs. 3, 4, and 5 were used to find the value of the unsigned difference in spontaneous curvature $|\Delta C_0|$ and/or the value of χ_{MF} that best fit the K_C data for all concentrations $\overline{\phi}$. Areas per lipid A_L (shown in Table 1) were found in the literature at 37°C, except for POPA, which was recently obtained by MD simulation. Fits were obtained using Origin 2019 (Northampton, MA) with user-created non-linear least-squares fitting functions written in Python.

RESULTS

Results for K_C for mixtures of four pairs of lipids are shown in Fig. 2. The fitted solid curves minimize the sum of squares for the five data points. The dashed K_D olive lines linearly connect the ends of the solid curves that obtain the best fitted values of K_C to the data. The data in Fig. 2 are qualitatively consistent with diffusional softening occurring in bilayers consisting of mixtures of lipids that have different spontaneous curvatures.

This qualitative consistency led us to extract quantitative results for the spontaneous lipid curvature from these equilibrium data. Let us focus here on POPC/POPE. We first consider using a literature value $|\Delta C_0| = 0.327$ nm^{-1} obtained from $C_0 = -0.317$ nm^{-1} for POPE (45) and $C_0 = +0.01$ nm^{-1} for POPC (14). We also initially constrained $\chi_{MF} = 0$ because that is what previous theory assumed. The fit (Fig. 3, *magenta short-dashed curve*) then finds K_C for all five data points including the single-component endpoints. This very poor fit with the large reduced chi-square of the fit (χ^2_{red}) of 7.6 recorded in Table 2 indicates that the assumed values of $|\Delta C_0| = 0.33$ nm^{-1} and $\chi_{MF} = 0$ are incorrect. That strong disagreement with the data is alleviated considerably by allowing $|\Delta C_0|$ to fit (Fig. 3, *dash-dot gray curve*), but the ensuing $|\Delta C_0|$ (0.81 nm^{-1}) is over twice as large as the H_{II} value of 0.33 nm^{-1} (46). A better fit is obtained by not constraining χ_{MF} while holding $|\Delta C_0|$ fixed (Fig. 3, *solid red curve*). Allowing both parameters to fit (*solid blue curve* in Fig. 3, also in Fig. 2 *B*) obtains $|\Delta C_0| = 0.44$ nm^{-1} with an uncertainty that includes the H_{II} value. Either of the two latter fits implies that a non-zero χ_{MF} is an important parameter for interpreting our data. The same kind of fit obtains even larger values of $|\Delta C_0|$ for the lipid pairs POPC/POPS and POPC/POPA—see Table 2.

Although the differences with the H_{II} value do fall within the experimental uncertainty for the POPC/POPE system, we are nevertheless concerned that our values of $|\Delta C_0|$ in Table 2 are rather large, even a bit larger than the reported spontaneous curvature of DOPE (0.41 nm^{-1}) (14). Observe, though, that the inferred values of $|\Delta C_0|$ for each binary system become smaller if we assume that our K_C values are too small by the same factor for all compositions. This does not change the values of α in Eqs. 3 and 4, because K_C and K_D change in the same proportion, but the factor of K_D in Eq. 4 forces a decrease in $|\Delta C_0|$ to maintain the same values of α. There is indeed a good justification for increasing the values of K_C in Fig. 2 and, thereby, those of K_D, because those values were obtained from the XDS data using a fitting program that does not include the effect of tilt. Much of the data in this study were not of high enough quality to fit with the additional parameter that accounts for tilt, but for high-quality POPC data, the inclusion of tilt was previously shown to increase the bending modulus by a factor of 1.33 (47). Applying this factor to the present data in Fig. 2 yields the results in the $|\Delta C_0|^{\#}$ column in Table 2. Even with that increase, GUV results for the closely similar 1-stearoyl-2-oleoyl-*sn*-glycero-3-phosphocholine (SOPC) lipid are greater by a factor of about 1.22 (47). In the discussion section, we will offer a rationale for why this second factor might additionally have to be applied to the bending moduli in Fig. 2, and the $|\Delta C_0|^{\&}$ column in Table 2 shows the result of doing so.

Regardless of these nuances, a main result is that a mean field term is required to obtain differences in the intrinsic lipid curvature of the POPC/POPE binary mixture that are consistent with previous H_{II} results.

TABLE 1 Area per lipid, A_L

Lipid	Ref.	A_L (Å^2)
POPC	Kučerka et al. (44)	66.5
POPS	Kučerka et al. (44)	64.5
POPE	Kučerka et al. (44)	58.5
POPA	[a]	58.0
DLPC	Kučerka et al. (44)	62.0
DiPhyPC	Tristram-Nagle et al. (1)	81.9

A_L values used in Eq. 4 were reported at 37°C.
[a]J. Klauda at University of Maryland, personal communication, August 2025.

DISCUSSION

Putting aside the finer points in the preceding section, there is an important comparison to GUV data that pertains to mixtures. Sapp et al. (25) found, using GUVs, that the equilibrium K_C was reduced when 40% DOPE was added to POPC, but only by 24%, corresponding to $K_C/K_D = 0.76$. Since POPE would be assumed to have smaller negative curvature than DOPE, one would expect our decrease in K_C for POPE in POPC to be smaller than 24% instead of the interpolated ≈50% from Fig. 3, so there would apparently be strong disagreement. Similarly, addition of HIV fusion peptide FP23 resulted in a greater decrease in K_C when measured in stacks by XDS than when measured in GUVs (48).

We suggest an explanation for the behavior in the preceding paragraph that involves interactions and the different length scales of the measurements. The equilibrium GUV analysis uses low q modes that have wavelengths on the order of a micrometer. In contrast, the XDS data come from q values that correspond to a 3- to 30-nm length scale range. The GUV result gives $|\Delta C_0| = 0.37$ nm^{-1}, in reasonable agreement with the H_{II} result of 0.41 nm^{-1} (14), provided χ_{MF} is assumed to be 0, and it would be even smaller for larger

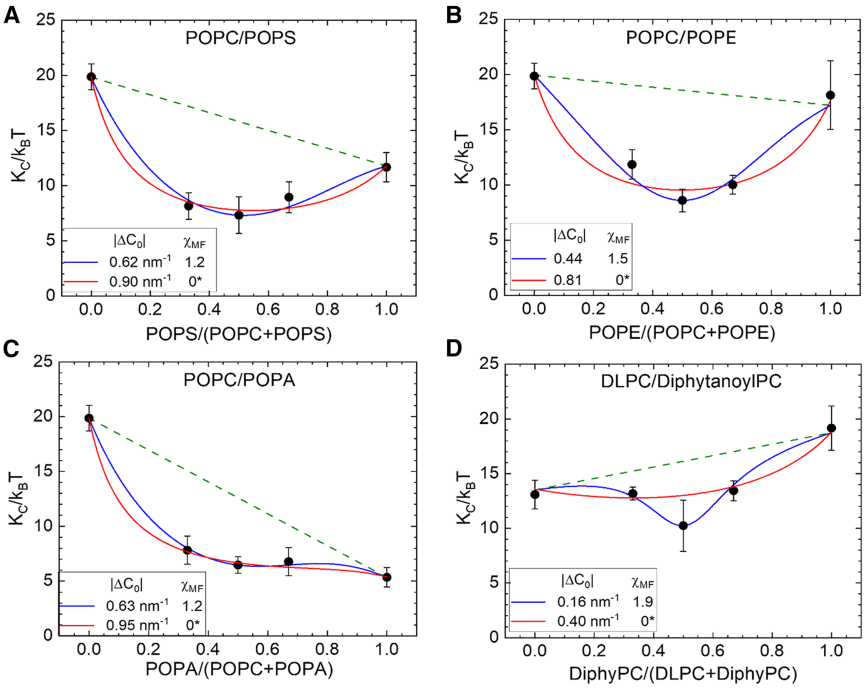

FIGURE 2 The bending modulus K_C (*solid circles*) versus mole fraction $\overline{\phi}$ for four different lipid mixtures: (*A*) POPC/POPS, (*B*) POPC/POPE, (*C*) POPC/POPA, and (*D*) DLPC/DiPhyPC. The solid curves are calculated from Eqs. 3 and 4 using the $|\Delta C_0|$ and χ_{MF} values shown in the legends that were obtained from the best fit to the five data points. The straight dashed olive lines show K_D from Eq. 5. Parameter values with an asterisk in the legend were fixed. The error bars on the experimental data points were obtained by fitting 3-9 XDS images at each mole fraction.

positive χ_{MF}. In contrast, to obtain spontaneous curvatures closer to the H_{II} result of 0.33 nm^{-1} for POPC/POPE requires $\chi_{MF} = 1.51$ in Table 2. To reconcile these results, we suggest that χ_{MF} should indeed be larger for mixtures at the short length scale of XDS than at the long length scale of GUVs. Local interactions between lipids have a short length scale that enhances local undulations, as indicated in Fig. 1, which would decrease the bending modulus at the XDS length scale. In contrast, local perturbations would not affect the amplitudes of long-wavelength undulations and the value of the GUV bending modulus.

It is also noteworthy that there is a similar trade-off in the length scales of GUVs versus XDS stacks when the tilt degree of freedom (49) is considered. The tilt spectrum scales as $1/q^2$, which has a negligible effect on the observed low q GUV modes, but it affects the spectrum for the high q modes (50) analyzed by XDS (49), with a crossover between the

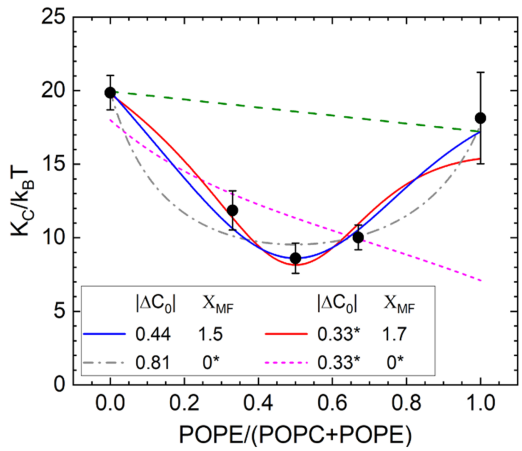

FIGURE 3 Calculated curves used different values of the $|\Delta C_0|$ (nm^{-1}) and χ_{MF} parameters shown in the legend. Parameter values with an asterisk in the legend were fixed. Data and K_D as in Fig. 2 *B*, but note that each of the fits has a different K_D line (not shown) that linearly connects the endpoints of the fitted curves. The error bars on the experimental data points were obtained by fitting 3-9 XDS images at each mole fraction.

TABLE 2 Summary of fitted parameters

Lipid mixture	χ_{MF}	$\|\Delta C_0\|$ (nm^{-1})	$\|\Delta C_0\|^{\#}$ (nm^{-1})	$\|\Delta C_0\|^{\&}$ (nm^{-1})	χ^2_{red}
POPC/POPE	1.51 (0.44)	0.44 (0.17)	0.38 (0.14)	0.35 (0.13)	1.30
POPC/POPE	1.73 (0.07)	0.33*	0.29*	0.26*	1.15
POPC/POPE	0*	0.81 (0.08)	0.71 (0.07)	0.64 (0.06)	1.27
POPC/POPE	0*	0.33*	0.29*	0.26*	7.63
POPC/POPS	1.15 (1.45)	0.62 (0.44)	0.54 (0.38)	0.49 (0.35)	0.70
POPC/POPS	0*	0.89 (0.06)	0.77 (0.05)	0.70 (0.05)	0.40
POPC/POPA	1.17 (0.35)	0.63 (0.12)	0.55 (0.10)	0.49 (0.09)	0.07
POPC/POPA	0*	0.95 (0.03)	0.82 (0.03)	0.75 (0.02)	0.12
DLPC/DiPhyPC	1.86 (0.12)	0.16 (0.05)	0.14 (0.04)	0.13 (0.04)	0.66
DLPC/DiPhyPC	0*	0.41 (0.08)	0.36 (0.07)	0.32 (0.06)	1.06
DLPC/DiPhyPC	0.88 (0.49)	0.33*	0.29*	0.26*	0.96

χ_{MF} is the mean field parameter for the interaction energy between unlike lipids. $|\Delta C_0|$ is the unsigned unadjusted difference in spontaneous curvature between the two lipids, $|\Delta C_0|^{\#}$ is the value adjusted for tilt, and $|\Delta C_0|^{\&}$ is the value additionally adjusted to match GUV moduli. χ^2_{red} is the reduced chi-square of the fit. Uncertainties are in parentheses. An asterisk (*) indicates a fixed parameter.

two regimes. We suggest that the spectrum for short-range interactions in mixtures is even less dependent upon q than that for tilt (unless we are very close to the critical point of demixing), so again, there would be a crossover with small q modes analyzed for GUVs affected mostly by K_C and larger q modes affected also by local roughness due to compositional variations. Furthermore, the interaction between bilayers in our samples further suppresses the undulation spectrum, which would enhance the relative effect of the interactions.

Much as we would have liked XDS to be the preferred method to obtain spontaneous curvature directly on lipid bilayers, analysis of mixtures in GUVs appears to be the more direct method. Then, with values of $|\Delta C_0|$ from GUVs in hand, XDS would provide information via χ_{MF} about the lateral interactions between the lipids. Our treatment of interactions is technically equivalent to a mean field theory. An improved theory would combine the continuum level Helfrich-Canham energy, which for stacks of symmetric membranes is given by Eqs. 1 and 2, with a more local nearest-neighbor or short-range interaction. The requisite statistical thermodynamic treatment is beyond the scope of this paper, and it may be quite difficult to develop. In its absence, the standard χ_{MF} term summarily approximates enhanced non-ideality at the local level.

However, aside from (25), there are rather few results in the GUV literature regarding the effect of mixing lipids on the bending modulus. When small concentrations of negatively charged POPG were added to POPC GUVs, K_C increased by nearly a factor of 2 and then remained large up to pure POPG (30); this is the opposite of what diffusional softening predicts, as it has all the K_C values for mixtures above the interpolated K_D line; interestingly, this behavior was explained by theories of the electric double layer of a charged membrane on its curvature elastic response. By contrast, only 10% of the negatively charged glycolipid GM1 softens POPC membranes by about a factor of 4 (26), even more than our results for POPS and POPA in POPC/POPS and POPC/POPA mixtures, but the endpoint of pure GM1 was not studied.

Let us compare our results with the H_{II} literature results. In this discussion, we will make the conventional assumptions. 1) Additivity as described in the introduction is assumed. In particular, it is assumed that $|\Delta C_0|$ for two planar forming lipids is the same as given in the literature, even though each of those was obtained with a host H_{II}-forming lipid, usually DOPE. 2) The difference in spontaneous curvatures of two lipids does not depend upon the concentration. This is also essential for our analysis using Eq. 4. However, if a better theory predicts a concentration-dependent functional form, our data could equally well be fit to that.

We have already made detailed numerical comparisons for our POPE/POPC mixtures. It has been well documented that phosphoethanolamine (PE) lipids have large negative curvatures and that phosphocholine (PC) lipids have much smaller, nearly zero, spontaneous curvatures (51). We would like to note, however, that the difference is often explained by the smaller PE headgroup to give them a cone shape relative to a more cylindrical shape for PC lipids (4). That explanation implicates steric repulsive headgroup interactions. Gel-phase studies show that steric interactions are responsible for chain tilt in saturated PC lipids, but with a steric area of only 0.48 nm^2 (52), and the PE steric area is only about 0.40 nm^2, consistent with its untilted gel-phase hydrocarbon chains. Even the PC steric headgroup area is far smaller than the fluid areas in Table 1, which come about because of the disordering of the hydrocarbon chains, after which steric headgroup interactions are irrelevant. Instead, smaller areas (and higher transition temperatures) in PE lipids would be due to weak and transient hydrogen bonding between the amino nitrogen on one lipid and a phosphate oxygen of a neighbor (53). Hydrogen bonding has also been implicated recently in the context of diffusional softening (11).

Turning to the charged lipid mixtures, POPA and POPS are both negatively charged and both would also be conducive to hydrogen bonding—obviously so in the case of POPS, but also for POPA because the phosphates become partially protonated, which enables H-bond formation between neighboring phosphates (54). It may also be noted that hydrogen bonding in POPA is consistent with its smaller area in Table 1. Although we could find no literature results for C_0 for POPS or POPA, the preponderance of results for DOPS and DOPA are for negative C_0 (51). This would then require the H-bond attractive energy $e_{hb} < 0$ to have larger magnitude than the repulsive electrostatic energy $e_{el} > 0$. This is also consistent with our positive values of χ_{MF}, which are given by $\chi_{MF} = e_{AB} - \frac{1}{2}(e_{AA} + e_{BB})$, where we assign A to the charged lipid and B to POPC, and the e values are scaled by k_BT. The only non-zero term is e_{AA} because the chains are the same on POPC, POPS, and POPA, and there are no hydrogen bonds or electrostatic interactions involving POPC. Then $\chi_{MF} = -\frac{1}{2}e_{AA} = -\frac{1}{2}(e_{hb} + e_{el})$ just for the POPS and POPA lipids. Our result is that χ_{MF} is greater than 0, consistent with a stronger attractive H-bond interaction than the repulsive electrostatic interaction, $|e_{hb}| > |e_{el}|$.

It is also interesting to compare our values of $|\Delta C_0|$ for POPS and POPA in POPC with its negligible curvature to H_{II} values for C_0 for DOPS and DOPA, noting that the DO chains would tend to make C_0 more negative than the PO chains. Our $|\Delta C_0|^{\&}$ results (Table 2) with non-zero χ_{MF} are consistent with one H_{II} method, which reported about -0.4 nm^{-1} for both DOPS and DOPA (55). However, there are data that do not agree. Fuller et al. (56) reported a positive spontaneous curvature ($+0.07$ nm^{-1}) for DOPS (Na^+ counterion) when no salt was added, which turned to negative curvature when salt was added, presumably due to additional screening of the charged headgroup repulsive

interaction. Our experiments with POPS had only the Na^+ counterions and no added salt. Similarly, it was reported that C_0 for DOPA is only -0.08 nm^{-1} in water, decreasing to -0.23 nm^{-1} as salt was added (57).

Turning finally to DiPhyPC/DLPC mixtures, the branched DiPhyPC chains should broaden the chain region relative to the PC headgroup, consistent with its much larger area per headgroup in Table 1, leading to more negative C_0 compared to unbranched chains. The H_{II} curvatures are -0.21 ± 0.01 nm^{-1} for DiPhyPC and 0.11 ± 0.05 nm^{-1} for DLPC (14). This gives a difference 0.33 ± 0.06 nm^{-1} that is larger than our $|\Delta C_0|^{\&} = 0.13 \pm 0.04$ nm^{-1} in Table 2 when we allowed both spontaneous curvature and χ_{MF} to fit. Curiously, $|\Delta C_0|^{\&}$ was about the same when χ_{MF} was constrained to zero. Perhaps most importantly, χ_{MF} was positive whether spontaneous curvature was held fixed or not, which is consistent with an excess attractive energy between the phytanoyl chains due to favorable knobs in hole packing.

Let us finally come back to discuss the second factor that we use to bring our values of the bending moduli to match those from GUVs. As noted earlier, there is a modest factor of about 1.22 greater bending modulus for SOPC single-component GUV bilayers, even when tilt was included in the analysis of XDS data (47). The question now is whether such a factor should generally be applied to our XDS bending moduli to make them agree with those from GUVs or if the inverse factor should be applied to the GUV moduli, an issue that has been unresolved. Applying only the factor due to tilt to our K_C, our $|\Delta C_0|^{\#}$ for the POPC/POPE mixture would have been a higher 0.38 nm^{-1}, further from the H_{II} value 0.33 nm^{-1} than the $|\Delta C_0|^{\&} = 0.35$ nm^{-1} shown in Table 2 for which the 1.22 factor was applied. Because uncertainties are rather large, consistency of the XDS values with the H_{II} value would only slightly favor increasing our XDS values of K_C to better match the GUV value. However, this choice is consistent with both GUV analysis and the very definition of K_C focusing on the long length scale represented by Eq. 1, whereas the shorter XDS length scale might include additional short-range fluctuations—perhaps protrusions—or it might reflect the fact that the interaction between bilayers in the sample stack is approximated by a harmonic potential in our fitting program. More generally, this is an example where obtaining consistency between one membrane property, $|\Delta C_0|$ in this case, could be helpful in resolving differences between experimental methods involving another property, K_C in this case.

CONCLUSIONS

The apparent bending moduli (K_C) of fluid-phase bilayers consisting of binary mixtures of phospholipids with differing spontaneous curvatures (ΔC_0), POPC/POPE, POPC/POPA, POPC/POPS, and DLPC/DiPhyPC, were measured using XDS. Measurements were taken at five concentrations, covering the full range between the two pure lipids. While our data qualitatively conform to the predictions of diffusional softening for all four mixtures, when we extract differences in spontaneous curvature using previous theory, there is a quantitative mismatch for POPC/POPE with results from H_{II} and GUV studies. A new modified equation describing diffusional softening is presented that includes a mean field parameter χ_{MF} to account for interactions between lipids. When that equation was used to fit the K_C data with spontaneous curvature and χ_{MF} as free parameters, much better agreement was obtained with earlier results for ΔC_0. Further comparison to GUV measurements suggest there is an effect beyond diffusional softening that is lowering apparent K_C values as measured by XDS. We suggest that short-range interaction-induced roughness is more significant at the short length scales measured by XDS than at the longer length scales measured in GUVs. This hypothesis could not be quantitatively evaluated, as mean field theory does not account for local correlations. The study has some experimental limitations: the limited number of usable XDS images at some concentrations resulted in greater experimental uncertainties, which in turn affected the uncertainties for $|\Delta C_0|$ and χ_{MF}; pure POPE also proved difficult to hydrate fully. There are several interesting avenues for future work. A model could be developed to better capture short-range correlations by mixing the continuum-level Helfrich-Canham energy with a more local interaction energy. In addition, GUV measurements of spontaneous curvature could be used in combination with XDS to gain greater insight into lateral interactions between lipids.

DATA AND CODE AVAILABILITY

The XDS scattering data presented here have not been deposited in a public repository because they are not structural data, such as crystallographic data. The XDS data herein provide material moduli as well as structural data, and these moduli are presented in this paper. The obtained structural data will be deposited at the time of their publication in the future. These XDS data will not be shared publicly until the structural part is published. However, they may be shared privately upon reasonable request.

ACKNOWLEDGMENTS

We are grateful to Vadim Frolov, Frank Brown, Sol Gruner, Georg Pabst, and Alex Sodt for insightful comments. This work is based on research conducted at the Center for High Energy X-ray Sciences (CHEXS at CHESS), which is supported by the National Science Foundation under award DMR-1829070, and the Macromolecular Diffraction at CHESS (MacCHESS) facility, which is supported by award 1-P30- GM124166-01A1 from the National Institute of General Medical Sciences, National Institutes of Health and the New York State's Empire State Development Corporation (NYSTAR). The authors would also like to acknowledge Dr. Stephen Paul Meisburger for his help at CHEXS (CHESS) and Rohan Rarasnis for help with the CHESS data collection. Additional support for this work was from the National Institute of Allergy and Infectious Diseases (NIAID) 1-R01AI172861 (S.T.-N.), the National Science Foundation (NSF) CHE-2514495 (M.D. and P.W.), the Department of

Commerce Award 70NANB24H248 (M.D.), and the NASA Pennsylvania Space Grant Consortium (L.K.).

AUTHOR CONTRIBUTIONS

S.T.-N. and J.F.N. designed the research; S.T.-N. supervised the collection of XDS data at CHESS; L.K. and S.T.-N. analyzed the experimental data; M.D. and P.W. developed the MF theory in supporting material; and S. T.-N., J.F.N., and M.D. wrote the paper with support from L.K. and P.W.

DECLARATION OF INTERESTS

The authors declare no competing interests.

SUPPORTING MATERIAL

Supporting material can be found online at https://doi.org/10.1016/j.bpj.2025.12.037.

REFERENCES

1. Tristram-Nagle, S., D. J. Kim, …, J. F. Nagle. 2010. Structure and water permeability of fully hydrated diphytanoylPC. *Chem. Phys. Lipids.* 163:630–637. https://doi.org/10.1016/j.chemphyslip.2010.04.011.
2. Greenwood, A. I., S. Tristram-Nagle, and J. F. Nagle. 2006. Partial molecular volumes of lipids and cholesterol. *Chem. Phys. Lipids.* 143:1–10. https://doi.org/10.1016/j.chemphyslip.2006.04.002.
3. Pan, J., S. Tristram-Nagle, and J. F. Nagle. 2009. Effect of cholesterol on structural and mechanical properties of membranes depends on lipid chain saturation. *Phys. Rev.* 80:021931. https://doi.org/10.1103/PhysRevE.80.021931.
4. Israelachvili, J. N., S. Marcelja, and R. G. Horn. 1980. Physical principles of membrane organization. *Q. Rev. Biophys.* 13:121–200. https://doi.org/10.1017/S0033583500001645.
5. Bashkirov, P. V., K. V. Chekashkina, …, V. A. Frolov. 2011. Variation of lipid membrane composition caused by strong bending. *Biochem. Moscow. Suppl. Ser. A.* 5:205–211. https://doi.org/10.1134/S1990747811101003x.
6. Baumgart, T., B. R. Capraro, …, S. L. Das. 2011. Thermodynamics and mechanics of membrane curvature generation and sensing by proteins and lipids. *Annu. Rev. Phys. Chem.* 62:483–506. https://doi.org/10.1146/annurev.physchem.012809.103450.
7. Gruner, S. M., V. A. Parsegian, and R. P. Rand. 1986. Directly measured deformation energy of phospholipid H-II hexagonal phases. *Faraday Discuss.* 81:29–37. https://doi.org/10.1039/dc9868100029.
8. Rand, R. P., and V. A. Parsegian. 1997. Hydration, curvature, and bending elasticity of phospholipid monolayers. *Lipid Polymorphism and Membrane Properties.* 44:167–189. https://doi.org/10.1016/S0070-2161(08)60208-7.
9. Gawrisch, K., V. A. Parsegian, …, R. P. Rand. 1992. Energetics of a hexagonal lamellar hexagonal-phase transition sequence in dioleoylphosphatidylethanolamine membranes. *Biochemistry.* 31:2856–2864. https://doi.org/10.1021/bi00126a003.
10. Rand, R. P., N. L. Fuller, …, V. A. Parsegian. 1990. Membrane curvature, lipid segregation, and structural transitions for phospholipids under dual-solvent stress. *Biochemistry.* 29:76–87. https://doi.org/10.1021/bi00453a010.
11. Hossein, A., A. H. Beaven, …, A. J. Sodt. 2024. Softening in two-component lipid mixtures by spontaneous curvature variance. *J. Phys. Chem. B.* 128:6317–6326. https://doi.org/10.1021/acs.jpcb.3c08117.
12. Sodt, A. J., R. M. Venable, …, R. W. Pastor. 2016. Nonadditive compositional curvature energetics of lipid bilayers. *Phys. Rev. Lett.* 117:138104. https://doi.org/10.1103/PhysRevLett.117.138104.
13. Kaltenegger, M., J. Kremser, …, G. Pabst. 2021. Evidence for non-addititve intrinsic lipid curvature mixing of sphingolipids from X-ray experiments on inverted hexagonal phases. *European Biophysics Journal with Biophysics Letters.* 50:170.
14. Kaltenegger, M., J. Kremser, …, G. Pabst. 2021. Intrinsic lipid curvatures of mammalian plasma membrane outer leaflet lipids and ceramides. *Bba-Biomembranes.* 1863:183709. https://doi.org/10.1016/j.bbamem.2021.183709.
15. Leibler, S. 1986. Curvature instability in membranes. *J. Phys. France.* 47:507–516. https://doi.org/10.1051/jphys:01986004703050700.
16. Reister-Gottfried, E., S. M. Leitenberger, and U. Seifert. 2010. Diffusing proteins on a fluctuating membrane: Analytical theory and simulations. *Phys. Rev.* 81:031903. https://doi.org/10.1103/PhysRevE.81.031903.
17. Bashkirov, P. V., P. I. Kuzmin, …, V. A. Frolov. 2022. Molecular shape solution for mesoscopic remodeling of cellular membranes. *Annu. Rev. Biophys.* 51:473–497. https://doi.org/10.1146/annurev-biophys-011422-100054.
18. Tristram-Nagle, S., and J. F. Nagle. 2007. HIV-1 fusion peptide decreases bending energy and promotes curved fusion intermediates. *Biophys. J.* 93:2048–2055. https://doi.org/10.1529/biophysj.107.109181.
19. Tristram-Nagle, S., R. Chan, …, J. F. Nagle. 2010. HIV fusion peptide penetrates, disorders, and softens T-cell membrane mimics. *J. Mol. Biol.* 402:139–153. https://doi.org/10.1016/j.jmb.2010.07.026.
20. Illya, G., R. Lipowsky, and J. C. Shillcock. 2006. Two-component membrane material properties and domain formation from dissipative particle dynamics. *J. Chem. Phys.* 125:114710. https://doi.org/10.1063/1.2353114.
21. Imparato, A., J. C. Shillcock, and R. Lipowsky. 2005. Shape fluctuations and elastic properties of two-component bilayer membranes. *Europhys. Lett.* 69:650–656. https://doi.org/10.1209/epl/i2004-10382-3.
22. Lessen, H. J., K. C. Sapp, …, A. J. Sodt. 2022. Molecular mechanisms of spontaneous curvature and softening in complex lipid bilayer mixtures. *Biophys. J.* 121:3188–3199. https://doi.org/10.1016/j.bpj.2022.07.036.
23. Pöhnl, M., M. F. W. Trollmann, and R. A. Böckmann. 2023. Nonuniversal impact of cholesterol on membranes mobility, curvature sensing and elasticity. *Nat. Commun.* 14:8038. https://doi.org/10.1038/s41467-023-43892-x.
24. Brannigan, G., and F. L. H. Brown. 2005. Composition dependence of bilayer elasticity. *J. Chem. Phys.* 122:074905. https://doi.org/10.1063/1.1851983.
25. Sapp, K., M. Aleksanyan, …, A. Sodt. 2023. Kinetic relaxation of giant vesicles validates diffusional softening in a binary lipid mixture. *Phys. Rev. E.* 107:054403. https://doi.org/10.1103/PhysRevE.107.054403.
26. Fricke, N., and R. Dimova. 2016. GM1 softens POPC membranes and induces the formation of micron-sized domains. *Biophys. J.* 111:1935–1945. https://doi.org/10.1016/j.bpj.2016.09.028.
27. Fiorin, G., L. R. Forrest, and J. D. Faraldo-Gómez. 2023. Membrane free-energy landscapes derived from atomistic dynamics explain nonuniversal cholesterol-induced stiffening. *PNAS Nexus.* 2:pgad269. https://doi.org/10.1093/pnasnexus/pgad269.
28. Mercker, M., M. Ptashnyk, …, W. Jäger. 2012. A multiscale approach to curvature modulated sorting in biological membranes. *J. Theor. Biol.* 301:67–82. https://doi.org/10.1016/j.jtbi.2012.01.039.
29. Gupta, S., J. Soni, …, T. Mandal. 2023. Origin of the nonlinear structural and mechanical properties in oppositely curved lipid mixtures. *J. Chem. Phys.* 159:165102. https://doi.org/10.1063/5.0167144.
30. Faizi, H. A., S. L. Frey, …, P. M. Vlahovska. 2019. Bending rigidity of charged lipid bilayer membranes. *Soft Matter.* 15:6006–6013. https://doi.org/10.1039/c9sm00772e.
31. Tristram-Nagle, S. A. 2007. Preparation of oriented, fully hydrated lipid samples for structure determination using X-ray scattering. *Methods Mol. Biol.* 400:63–75. https://doi.org/10.1007/978-1-59745-519-0_5.

32. Mitra, S., M. T. Chen, …, S. Tristram-Nagle. 2025. Cyclization of two antimicrobial peptides improves their activity. *ACS Omega.* 10:9728–9740. https://doi.org/10.1021/acsomega.4c11466.

33. Lyatskaya, Y., Y. Liu, …, J. F. Nagle. 2001. Method for obtaining structure and interactions from oriented lipid bilayers. *Phys. Rev. E - Stat. Nonlinear Soft Matter Phys.* 63:011907. https://doi.org/10.1103/PhysRevE.63.011907.

34. Liu, Y., and J. F. Nagle. 2004. Diffuse scattering provides material parameters and electron density profiles of biomembranes. *Phys. Rev. E - Stat. Nonlinear Soft Matter Phys.* 69:040901. https://doi.org/10.1103/PhysRevE.69.040901.

35. Lei, N., C. R. Safinya, and R. F. Bruinsma. 1995. Discrete harmonic model for stacked membranes - Theory and experiment. *J. Phys. II France.* 5:1155–1163. https://doi.org/10.1051/jp2:1995174.

36. Dimova, R. 2014. Recent developments in the field of bending rigidity measurements on membranes. *Adv. Colloid Interface Sci.* 208:225–234. https://doi.org/10.1016/j.cis.2014.03.003.

37. Rawicz, W., K. C. Olbrich, …, E. Evans. 2000. Effect of chain length and unsaturation on elasticity of lipid bilayers. *Biophys. J.* 79:328–339. https://doi.org/10.1016/S0006-3495(00)76295-3.

38. Cuvelier, D., I. Derényi, …, P. Nassoy. 2005. Coalescence of membrane tethers:: experiments, theory, and applications. *Biophys. J.* 88:2714–2726. https://doi.org/10.1529/biophysj.104.056473.

39. Singh, P., P. Mahata, …, S. L. Das. 2012. Curvature sorting of proteins on a cylindrical lipid membrane tether connected to a reservoir. *Phys. Rev.* 85:051906. https://doi.org/10.1103/PhysRevE.85.051906.

40. Nagle, J. F. 2021. Measuring the bending modulus of lipid bilayers with cholesterol. *Phys. Rev. E.* 104:044405. https://doi.org/10.1103/PhysRevE.104.044405.

41. Pan, J., S. Tristram-Nagle, …, J. F. Nagle. 2008. Temperature dependence of structure, bending rigidity, and bilayer interactions of dioleoylphosphatidylcholine bilayers. *Biophys. J.* 94:117–124. https://doi.org/10.1529/biophysj.107.115691.

42. Heinrich, F., and J. F. Nagle. 2025. The effect of cholesterol on the bending modulus of DOPC bilayers: re-analysis of NSE data. *Soft Matter.* 21:2258–2267. https://doi.org/10.1039/d4sm01312c.

43. Frewein, M. P. K., P. Piller, …, G. Pabst. 2023. Distributing aminophospholipids asymmetrically across leaflets causes anomalous membrane stiffening. *Biophys. J.* 122:2445–2455. https://doi.org/10.1016/j.bpj.2023.04.025.

44. Kučerka, N., B. van Oosten, …, J. Katsaras. 2015. Molecular structures of fluid phosphatidylethanolamine bilayers obtained from simulation-to-experiment comparisons and experimental scattering density profiles. *J. Phys. Chem. B.* 119:1947–1956. https://doi.org/10.1021/jp511159q.

45. Frewein, M. P. K., M. Rumetshofer, and G. Pabst. 2019. Global small-angle scattering data analysis of inverted hexagonal phases. *J. Appl. Crystallogr.* 52:403–414. https://doi.org/10.1107/S1600576719002760.

46. Kollmitzer, B., P. Heftberger, …, G. Pabst. 2013. Monolayer spontaneous curvature of raft-forming membrane lipids. *Soft Matter.* 9:10877–10884. https://doi.org/10.1039/c3sm51829a.

47. Nagle, J. F. 2017. Experimentally determined tilt and bending moduli of single-component lipid bilayers. *Chem. Phys. Lipids.* 205:18–24. https://doi.org/10.1016/j.chemphyslip.2017.04.006.

48. Shchelokovskyy, P., S. Tristram-Nagle, and R. Dimova. 2011. Effect of the HIV-1 fusion peptide on the mechanical properties and leaflet coupling of lipid bilayers. *New J. Phys.* 13:025004. https://doi.org/10.1088/1367-2630/13/2/025004.

49. Jablin, M. S., K. Akabori, and J. F. Nagle. 2014. Experimental support for tilt-dependent theory of biomembrane mechanics. *Phys. Rev. Lett.* 113:248102. https://doi.org/10.1103/PhysRevLett.113.248102.

50. May, E. R., A. Narang, and D. I. Kopelevich. 2007. Role of molecular tilt in thermal fluctuations of lipid membranes. *Phys. Rev.* 76:021913. https://doi.org/10.1103/PhysRevE.76.021913.

51. Dymond, M. K. 2021. Lipid monolayer spontaneous curvatures: A collection of published values. *Chem. Phys. Lipids.* 239:105117. https://doi.org/10.1016/j.chemphyslip.2021.105117.

52. Tristram-Nagle, S., R. Zhang, …, J. F. Nagle. 1993. Measurement of chain tilt angle in fully hydrated bilayers of gel phase lecithins. *Biophys. J.* 64:1097–1109. https://doi.org/10.1016/S0006-3495(93)81475-9.

53. Nagle, J. F. 1980. Theory of the main lipid bilayer phase-transition. *Annu. Rev. Phys. Chem.* 31:157–196. https://doi.org/10.1146/annurev.pc.31.100180.001105.

54. Mille, M. 1981. Effect of nearest-neighbor interactions on surface titrations. *J. Colloid Interface Sci.* 81:169–179. https://doi.org/10.1016/0021-9797(81)90314-3.

55. Dymond, M. K., R. J. Gillams, …, G. S. Attard. 2016. Lipid spontaneous curvatures estimated from temperature dependent changes in inverse hexagonal phase lattice parameters: Effects of metal cations. *Langmuir.* 32:10083–10092. https://doi.org/10.1021/acs.langmuir.6b03098.

56. Fuller, N., C. R. Benatti, and R. P. Rand. 2003. Curvature and bending constants for phosphatidylserine-containing membranes. *Biophys. J.* 85:1667–1674. https://doi.org/10.1016/S0006-3495(03)74596-2.

57. Kooijman, E. E., V. Chupin, …, P. R. Rand. 2005. Spontaneous curvature of phosphatidic acid and lysophosphatidic acid. *Biochemistry.* 44:2097–2102. https://doi.org/10.1021/bi0478502.

Biophysical Journal, Volume *125*

Supplemental information

Bending moduli of mixtures: Diffusional softening and interactions

Lucy Knox, Peter Winstel, Markus Deserno, John F. Nagle, and Stephanie Tristram-Nagle

Supplemental Information for the paper

"Bending moduli of mixtures: diffusional softening and interactions"

Lucy Knox, Peter Winstel, Markus Deserno, John F. Nagle, and Stephanie Tristram-Nagle

Department of Physics, Carnegie Mellon University, 5000 Forbes Ave, Pittsburgh, PA 15213, USA

Deriving the softening formula

We derive a new formula for the effective softening of a binary mixed lipid membrane's curvature modulus. It extends the expression shown for instance in Ref. [S1] in three ways:

1. we generalize to the case in which the two pure mixtures do not have the same bending rigidity;
2. we do not assume that the difference in spontaneous curvature between the two phases is small;
3. we include the possibility of non-ideal mixing in a simple mean-field way.

A minimal model for diffusional softening must account both for *curvature elasticity* and for *lipid mixing*. Assume that at the level of a *single leaflet* (subscript "m" for "monolayer") this free energy density can be written by a standard Helfrich expression amended by a composition-dependent free energy of mixing,

$$H_{\mathrm{m}}(C,\phi) = \frac{1}{2}K^{\mathrm{loc}}_{\mathrm{C,m}}(\boldsymbol{r})\big[C - C^{\mathrm{loc}}_0(\boldsymbol{r})\big]^2 + f(\phi)\;, \qquad \text{Eq.1}$$

where $C = c_1 + c_2$ is the local extrinsic curvature and $\phi = \phi(\boldsymbol{r})$ is the local mole fraction of one of the two components. Furthermore, $K^{\mathrm{loc}}_{\mathrm{C,m}}(\boldsymbol{r})$ and $C^{\mathrm{loc}}_0(\boldsymbol{r})$ are *local* values for the bending modulus and the spontaneous curvature of a *single leaflet*, respectively. They are local because they depend on the local composition $\phi(\boldsymbol{r})$ in a way we still need to specify. We set the surface tension to zero and ignore the Gaussian term. For the mixing free energy density we make a simple mean field ansatz

$$f(\phi) = \frac{k_{\mathrm{B}}T}{A_{\mathrm{L}}}\Big[\phi\log\phi + (1-\phi)\log(1-\phi) + \chi_{\mathrm{MF}}\,\phi(1-\phi)\Big]\;, \qquad \text{Eq.2}$$

where χ_{MF} is the "Bragg-Williams" or "Flory-Huggins" or simply "mean-field" mixing parameter, and A_{L} is the area per lipid.

We now need to decide how the local bending modulus $K^{\mathrm{loc}}_{\mathrm{C,m}}(\boldsymbol{r})$ and the local spontaneous curvature $C^{\mathrm{loc}}_0(\boldsymbol{r})$ depend on local composition. In the absence of any further knowledge, the simplest assumption to make is that they are simply linear interpolations:

$$C^{\mathrm{loc}}_0(\boldsymbol{r}) = C^{\mathrm{loc}}_0(\phi(\boldsymbol{r})) = C_{0,1}(1-\phi(\boldsymbol{r})) + C_{0,2}\,\phi(\boldsymbol{r})\;, \qquad \text{Eq. 3a}$$

$$K^{\mathrm{loc}}_{\mathrm{C,m}}(\boldsymbol{r}) = K^{\mathrm{loc}}_{\mathrm{C,m}}(\phi(\boldsymbol{r})) = K_{\mathrm{C,m},1}(1-\phi(\boldsymbol{r})) + K_{\mathrm{C,m},2}\,\phi(\boldsymbol{r})\;. \qquad \text{Eq. 3b}$$

If the mixed state has an average composition $\bar{\phi}$, and ϕ locally deviates from this, we can write

$$\phi(\boldsymbol{r}) = \bar{\phi} + \psi(\boldsymbol{r}) \qquad \text{Eq.4}$$

and then express Eqs. 3 in terms of the small local deviations $\psi(\boldsymbol{r})$:

$$C^{\mathrm{loc}}_0(\bar{\phi},\psi(\boldsymbol{r})) = C_{0,\mathrm{D}}(\bar{\phi}) + \Delta C_0\,\psi(\boldsymbol{r})\;, \qquad \text{Eq.5}$$

$$K^{\mathrm{loc}}_{\mathrm{C,m}}(\bar{\phi},\psi(\boldsymbol{r})) = K_{\mathrm{D,m}}(\bar{\phi}) + \Delta K_{\mathrm{C,m}}\,\psi(\boldsymbol{r})\;, \qquad \text{Eq.5b}$$

where average spontaneous curvatures or bending rigidities and their differences, *i. e.*, *quantities that are no longer position dependent*, are defined as

$$C_{0,\mathrm{D}}(\bar{\phi}) = (1-\bar{\phi})C_{0,1} + \bar{\phi}\, C_{0,2} \qquad\qquad \Delta C_0 = C_{0,2} - C_{0,1} \qquad \text{Eq.6a}$$

$$K_{\mathrm{D,m}}(\bar{\phi}) = (1-\bar{\phi})K_{\mathrm{C,m},1} + \bar{\phi}\, K_{\mathrm{C,m},2} \qquad\qquad \Delta K_{\mathrm{C,m}} = K_{\mathrm{C,m},2} - K_{\mathrm{C,m},1}\ . \qquad \text{Eq.6b}$$

Observe that the resulting Hamiltonian, while quadratic in C, is *cubic* in ψ. It takes its minimum, as a function of C, at $C_{\mathrm{min}} = C_0(\bar{\phi}, \psi)$. Regarding the composition field, we had already decided to expand around $\phi = \bar{\phi}$, meaning that ψ is our second small variable. This, incidentally, is *not* where the total minimum of the Hamiltonian is, which instead lies at $\phi_{\mathrm{min}} = \frac{1}{2}$. However, if we were to pick this expansion point instead, then ψ would not fluctuate around 0, as assumed above, but instead around $\frac{1}{2} - \bar{\phi}$. For consistency reasons we do not wish to mix two different expansion points, and so we will continue to expand the composition degree of freedom around $\phi = \bar{\phi}$. Doing so, we arrive at the following quadratic expansion of the composition-curvature Hamiltonian in terms of the local fields $C(\boldsymbol{r})$ and $\psi(\boldsymbol{r})$:

$$H^{(2)}_{\mathrm{m}}(C,\psi) = \frac{1}{2}K_{\mathrm{D,m}}(\bar{\phi})\big(C - \Delta C_0\,\psi\big)^2 + \frac{1}{2}k_\psi\psi^2 \ \ + \ \ \mathrm{const}(C,\psi) \ \ + \ \ \mathrm{lin}(C,\psi)\ , \qquad \text{Eq.7}$$

where we also defined the parameter

$$k_\psi = \frac{k_{\mathrm{B}}T}{A_{\mathrm{L}}}\left[\frac{1}{\bar{\phi}(1-\bar{\phi})} - 2\chi_{\mathrm{MF}}\right]\ . \qquad \text{Eq.8}$$

Henceforth we will ignore the terms that are constant or linear in either C or ψ in Eq.7, because they do not affect the fluctuating quantities we wish to calculate. Observe the two key changes compared to the Hamiltonian from Eq.1 we started with: first, the bending rigidity multiplying the quadratic curvature penalty is no longer a local modulus; instead, it it a *constant*—namely, the *linear interpolation* between the two endpoint rigidities $K_{\mathrm{C,m},1}$ and $K_{\mathrm{C,m},2}$ using the *average* mole fraction $\bar{\phi}$; and second, the free energy of mixing is reduced to its second order term in the expansion around $\phi = \bar{\phi}$.

To transition from a monolayer to a bilayer, we add *two* such terms and flip the spontaneous curvature for the second one, because the second leaflet is flipped upside down. We also need to introduce two independent composition fluctuations $\psi_\pm$:

$$H(C,\psi_+,\psi_-) = \frac{1}{2}K_{\mathrm{D,m}}(\bar{\phi})\big(C - \Delta C_0\,\psi_+\big)^2 + \frac{1}{2}K_{\mathrm{D,m}}(\bar{\phi})\big(C + \Delta C_0\,\psi_-\big)^2 + \frac{1}{2}k_\psi({\psi^2}_+ + {\psi^2}_-)\ . \qquad \text{Eq.9}$$

In linear Monge gauge $h(\boldsymbol{r})$, the curvature can be written as $C = -\nabla^2 h(\boldsymbol{r})$, where ∇^2 is the base-plane Laplacian and $\boldsymbol{r} = (x,y) \in [0,L)^2$. Expanding the fields $h(\boldsymbol{r})$ and $\psi_\pm(\boldsymbol{r})$ in Fourier modes,

$$h(\boldsymbol{r}) = \sum_{\boldsymbol{q}} h_{\boldsymbol{q}}\ \mathrm{e}^{\mathrm{i}\boldsymbol{q}\cdot\boldsymbol{r}} \qquad , \qquad \psi_\pm(\boldsymbol{r}) = \sum_{\boldsymbol{q}} \psi_{\pm\boldsymbol{q}}\ \mathrm{e}^{\mathrm{i}\boldsymbol{q}\cdot\boldsymbol{r}}\ , \qquad \text{Eq.10}$$

we can derive after a short standard calculation that

$$H = L^2 \sum_{\boldsymbol{q}}\ \frac{1}{2}\boldsymbol{v}^\dagger_{\boldsymbol{q}}\mathbf{M}_{\boldsymbol{q}}\boldsymbol{v}_{\boldsymbol{q}}\ , \qquad \text{Eq.11}$$

where

$$\boldsymbol{v}_{\boldsymbol{q}} = \begin{pmatrix} h_{\boldsymbol{q}} \\ \psi_{+\boldsymbol{q}} \\ \psi_{-\boldsymbol{q}} \end{pmatrix} \quad \text{and} \quad \mathbf{M}_{\boldsymbol{q}} = \begin{pmatrix} 2K_{\mathrm{D,m}}q^4 & -K_{\mathrm{D,m}}q^2\,\Delta C_0 & K_{\mathrm{D,m}}q^2\,\Delta C_0 \\ -K_{\mathrm{D,m}}q^2\,\Delta C_0 & k_\psi + K_{\mathrm{D,m}}\,\Delta C_0^2 & 0 \\ K_{\mathrm{D,m}}q^2\,\Delta C_0 & 0 & k_\psi + K_{\mathrm{D,m}}\,\Delta C_0^2 \end{pmatrix} . \qquad \text{Eq.12}$$

Recall now the generalized equipartition theorem: a quadratic Hamiltonian $\frac{1}{2}\boldsymbol{x}^\dagger\mathbf{K}\boldsymbol{x}$ has the covariances

$$\beta\langle x_i x_j\rangle = (\mathbf{K}^{-1})_{ij} \ , \qquad \text{Eq.13}$$

where $\beta = 1/k_{\mathrm{B}}T$. Specifically calculating the hh-correlator, we find

$$\begin{aligned} \beta L^2\,\langle|h_{\boldsymbol{q}}|^2\rangle \;&=\; \frac{k_\psi + K_{\mathrm{D,m}}\,\Delta C_0^2}{2K_{\mathrm{D,m}}q^4(k_\psi + K_{\mathrm{D,m}}(\bar\phi)\,\Delta C_0^2) - 2(K_{\mathrm{D,m}}q^2\,\Delta C_0)^2} \\ &=\; \frac{k_\psi + K_{\mathrm{D,m}}\,\Delta C_0^2}{2K_{\mathrm{D,m}}q^4 k_\psi} \;=\; \frac{1}{K_{\mathrm{D}}q^4}\left[1 + \frac{K_{\mathrm{D}}\,\Delta C_0^2}{2k_\psi}\right] , \qquad \text{Eq.14} \end{aligned}$$

where in the last step we introduced the bilayer modulus $K_{\mathrm{D}}(\bar\phi) = 2K_{\mathrm{D,m}}(\bar\phi)$. Demanding that Eq.14 takes the classical form [bending modulus $\times\, q^4]^{-1}$ defines an *effective* $\bar\phi$-dependent bilayer bending rigidity $K_{\mathrm{C}}(\bar\phi)$, which is the one we measure:

$$\begin{aligned} \frac{K_{\mathrm{C}}(\bar\phi)}{K_{\mathrm{D}}(\bar\phi)} \;&=\; \left[1 + \frac{K_{\mathrm{D}}(\bar\phi)\,\Delta C_0^2}{2k_\psi}\right]^{-1} = \left[1 + \frac{K_{\mathrm{D}}(\bar\phi)\,\Delta C_0^2 A_{\mathrm{L}}\,\bar\phi(1-\bar\phi)}{2k_{\mathrm{B}}T\big[1 - 2\chi_{\mathrm{MF}}\bar\phi(1-\bar\phi)\big]}\right]^{-1} && \text{Eq.15a} \\ &\simeq 1 - \frac{K_{\mathrm{D}}(\bar\phi)\,\Delta C_0^2 A_{\mathrm{L}}\,\bar\phi(1-\bar\phi)}{2k_{\mathrm{B}}T\big[1 - 2\chi_{\mathrm{MF}}\bar\phi(1-\bar\phi)\big]} \qquad \Big(\text{if } A_{\mathrm{L}}\,\Delta C_0^2 \ll 1\Big) && \text{Eq.15b} \\ &= 1 - \frac{K_{\mathrm{D}}(\bar\phi)\,\Delta C_0^2 A_{\mathrm{L}}\,\bar\phi(1-\bar\phi)}{2k_{\mathrm{B}}T} \qquad \Big(\text{if additionally } \chi_{\mathrm{MF}} = 0\Big) . && \text{Eq.15c} \end{aligned}$$

Equation 15c is formula (Eqs.24,25) in the paper "Molecular mechanisms of spontaneous curvature and softening in complex lipid bilayer mixtures" by Sapp *et al.* [S1], except for the differences in notation we follow here and the fact that they have additional l-factors due to their treatment of the spherical case. Also, we here provide an explicit argument why the bare bending rigidity should be the linear interpolation between the two endpoint rigidities. Observe that there is no compelling reason to use the expansion for small cur-vature differences, since the original formula Eq.15a is not really any more complicated. Incidentally, an alternative way of writing that full answer is

$$\frac{1}{K_{\mathrm{C}}(\bar\phi)} - \frac{1}{K_{\mathrm{D}}(\bar\phi)} \;=\; \frac{\Delta C_0^2}{2k_\psi} \;=\; \frac{\Delta C_0^2 A_{\mathrm{L}}\,\bar\phi(1-\bar\phi)}{2k_{\mathrm{B}}T\big[1 - 2\chi_{\mathrm{MF}}\bar\phi(1-\bar\phi)\big]} . \qquad \text{Eq.15d}$$

Supplemental References

[S1] Sapp, K., M. Aleksanyan, K. Kerr, R. Dimova, and A. Sodt, 2023. Kinetic relaxation of giant vesicles validates diffusional softening in a binary lipid mixture. *Phys. Rev. E* 107:054403.

X-ray diffuse scattering experimental data

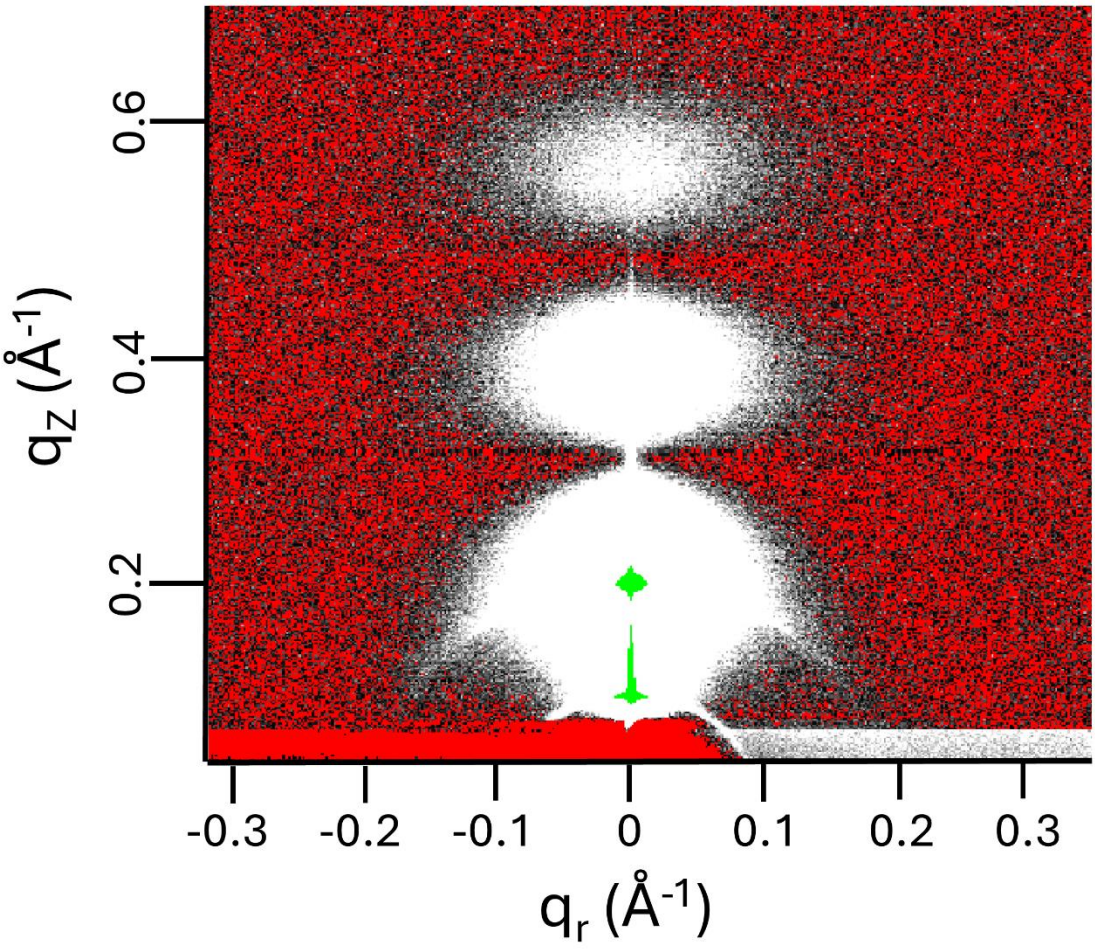

Figure S1. X-ray diffuse scattering (XDS) data collected at 37 °C at CHESS. The sample is DLPC/diphytanoylPC (1:1 molar ratio), D-spacing = 62 Å. Two backgrounds were subtracted: a negative background image to remove air, water and mylar scattering, followed by a flattening background to match the intensity underneath the diffuse lobes with the intensity on both sides of the lobes (see Materials and Methods). Red pixels indicate zero intensity. All images had two backgrounds subtracted this way before liquid crystal data analysis.